Elsevier Editorial System(tm) for Mechanics of Materials
Manuscript Draft

Manuscript Number:

Title: Size effects and temperature dependence on strain-hardening mechanisms in some face centered cubic materials

Article Type: Research Paper

Keywords: Size effects; Thermomechanical behaviour; Plasticity; Face centered cubic materials; Dislocations substructures; Strain gradient plasticity model

Corresponding Author: Prof. Eric Hug,

Corresponding Author's Institution: Laboratoire CRISMAT, UMR CNRS 6508

First Author: Eric Hug

Order of Authors: Eric Hug; Pierre-Antoine Dubos; Clément Keller; Laurent Duchêne; Anne-Marie Habraken

Manuscript Region of Origin: FRANCE

Suggested Reviewers: Brigitte Weiss
Vienna University
weissb@ap.univie.ac.at
Some of their works are concerning by size effects in metallic samples

Anders Jafors
Jöhnhöping University
anders.jarfors@jth.hj.se
Work in size effects in metallic alloys

Andrey Molotnikov
Monash University
andrey.molotnikov@monash.edu
Some of researchs deal with microforming of small metallic parts

philippe picart
Femto laboratory
philippe.picart@femto-st.fr
Researcher in microforming processes

Daniel Kiener
Loeben University
daniel.kiener@uniloeben.ac.at
Research interests in metallurgical aspects of miniaturization of metallic parts

Opposed Reviewers:

Cover letter

Dear Professor Nemat-Nasser,

Please find below the details of a manuscript we wish to submit for publication in Mechanics of Materials.

Sincerely Yours

E. Hug

Title page information

Paper title: Size effects and temperature dependence on strain-hardening mechanisms in some face-centered cubic materials

Authors: E. Hug[a], P.A. Dubos[a], C. Keller[b], L. Duchêne[c], A.M. Habraken[c]

Affiliations:

[a]Laboratoire CRISMAT/ENSICAEN/UCBN/CNRS, UMR 6508, 6 Bd du Maréchal Juin, 14050 Caen, FRANCE
[b]Groupe de Physique des Matériaux, INSA Rouen, Université de Rouen, CNRS UMR 6634, BP 08 Avenue de l'université, 76801 St. Etienne du Rouvray, France
[c]Département ArGEnCo, division MS^{2}F, Université de Liège, Chemin des Chevreuils 1, 4000 Liège, Belgique

Corresponding author:

Eric HUG, Professor
Laboratoire CRISMAT, Ensicaen, Université de Caen, CNRS,
6 Bd Maréchal Juin, 14050 Caen France.
Tel: +33 2 31 45 13 13
Fax: +33 2 31 95 16 00
e-mail: eric.hug@ensicaen.fr

Author statement

The authors declare that they have not submitted their paper for publication elsewhere, neither the paper, in its entirety, in part, or in a modified version, has been published elsewhere. All the results presented in this paper are new.

An expanded version a paper containing some parts of results has previously been submitted for possible publication in JMPS, but the editor encourages us to shorten it and submit the manuscript elsewhere.

Size effects and temperature dependence on strain-hardening mechanisms in some face centered cubic materials

E. Hug[a], P.A. Dubos[a], C. Keller[b], L. Duchêne[c], A.M. Habraken[c]

[a]Laboratoire de Cristallographie et Sciences des Matériaux, ENSICAEN, Université de Caen, CNRS, 6 Bd Maréchal Juin, 14050 Caen France

[b]Groupe de Physique des Matériaux, UMR 6634 CNRS - Université de Rouen, INSA de Rouen, avenue de l'université, 76800 Saint-Etienne du Rouvray, France

[c]Département ArGEnCo, division MS^{2}F, Université de Liège, Chemin des Chevreuils 1, 4000 Liège, Belgique

Abstract

The mechanical behaviour of face centered cubic metals is deeply affected when specimen dimensions decrease from a few millimeters to a few micrometers. At room temperature, a critical thickness (t) to grain size (d) ratio $(t/d)_c$ was previously highlighted, under which the softening of mechanical properties became very pronounced both in terms of Hall-Petch relation and work hardening mechanisms. In this work, new experimental results are provided concerning the influence of temperature on this size effect for copper, nickel and Ni-20wt.%Cr, representative of a wide range of deformation mechanisms (*i.e.* dislocation slip character). It is shown that multicrystalline samples ($t/d < (t/d)_c$) are not deeply affected by an increase in temperature, independently of the planar or wavy character of dislocation glide. For pronounced wavy slip character metals, surface effects in polycrystals ($t/d > (t/d)_c$) are not significant enough to reduce the gap between polycrystal and multicrystal mechanical behaviour when the temperature increases. However, a transition from wavy

slip to planar glide mechanisms induces a modification of the polycrystalline behaviour which tends toward multicrystalline one with a moderate increase in temperature. This work demonstrates that surface effects and grain size influence can be successfully disassociated for the three studied materials using an analysis supported by the Kocks-Mecking formalism. All these results are supported by microscopic investigations of dislocation substructures and compared to numerical simulations using a stress gradient plasticity model.

Keywords: Size effects; Thermomechanical behaviour; Plasticity; Face centered cubic materials; Dislocations substructures; Strain gradient plasticity model

1. Introduction

Designing small technical systems often means dealing with confined plasticity at scales below 10^{-4} m, which requires additional knowledge of the material work hardening properties. At macroscopic scale, for instance, micro-components working with metallic parts of typical dimensions in the range [1-500] μm are often processed by traditional ways: forging, rolling or extrusion processes [1]. For these forming processes, it is necessary to take into account the size effects [2] to correctly predict the force, the geometry, and the appearance of fracture or necking [3, 4]. However, the strong variability of the mechanical responses to the external loadings can imply a lack of reliability of these micro-systems [5]. This may lead to an early or unexpected failure due to the development of damage consecutive to their forming process [3, 6, 7].

Previous works have clearly shown a so-called "smaller is softer" trend for samples with critical dimensions in the range of 1 to 500 μm [8-12], triggered by the *t/d* parameter (*i.e.* the thickness (*t*) to grain size (*d*) ratio). When this parameter decreases, the flow stress, the hardening behaviour and the fracture strain of face centered cubic (fcc) metals are strongly modified as reported by numerous researchers both in terms of experimental studies [9-11, 13-15] and numerical simulations [4, 16]. This modification is observed either by changing grain size for constant thickness (deviation from the Hall-Petch relation for the larger grain size levels [17]) or by modifying the thickness for constant grain size [12, 18]. Three kinds of mechanical behaviour have been highlighted for fcc structure when the *t/d* ratio is reduced: polycrystalline, multicrystalline and quasi-single crystalline [17], separated by two critical *t/d* ratios [9]. The typical value $(t/d)_c$ separating the polycrystalline behaviour from the multycristalline one reported in the literature ranges between 3 and 15, mainly depending on the stacking-fault energy. The second critical *t/d* ratio separating the multicrystalline from the quasi-single crystalline behaviour is close to the unity.

The physical origin of this softening effect can be found in the surface effects occuring in multicrystalline samples during the strengthening. These surface effects involve a stress gradient between core and surface grains of around 30%, directly linked to the different mean dislocation cell size observed in these two regions, especially during the second work hardening stage for samples with *t/d* lower than $(t/d)_c$ [19]. Activating cross-slip mechanisms in the third work hardening stage leads to a progressive decrease of these stress gradient effects and therefore materials become less sensitive to size effects.

The transition from a polycrystalline to a quasi-single crystalline state modifies both mechanical behaviour and forming ability [20-23]. In order to improve the formability of micro components in the dimension range [1-500] μm, a moderate modification in temperature could be an interesting option. However, very few experimental data are available in literature concerning size effects and temperature. Eichenhueller and co-workers [24] studied the microforming of brass and stainless steel microparts from room temperature up to 673 K. They clearly show a homogenizing effect of the temperature on the main parameters of microforming processes as upsetting or extrusion. In a recent study devoted to copper for two extreme *t/d* values [25], one higher and the other below the critical value $(t/d)_c$, we reported that polycrystalline sample behaviour tends toward multicrystalline one with a moderate increase in temperature, approximately above a value of 373 K. These experimental results were correlated to the progressive predominance of the third work hardening stage and associated dislocation cross-slip. The origin of this phenomenon remains nevertheless unclear. Indeed, two mechanisms could be responsible for this observation: (i) a modification of the grain size dependence with a change in temperature, and (ii) a progressive generalization of surface effects in the entire volume of the samples even for polycrystalline samples. These two mechanisms may also act simultaneously.

The objective of this paper is, hence, to contribute to the understanding of the temperature dependence of the size effects in low dimension metallic samples. The contribution of the two mechanisms cited above will be analyzed for a large range of temperature and *t/d* values. Experimental results concerning size effects in a temperature range from 203 K to 773 K are presented for nickel, copper and Ni-20wt.%Cr alloy characterized by different slip character. The Hall-Petch relation, the

strain hardening and the free surface influence are experimentally investigated using a work hardening formalism based on Kocks-Mecking works which help to disassociate the grain size and surface effects. The discussion of these results is supported by two complementary tools. From a microstructural point of view, Transmission Electron Microscopy (TEM) observations are performed in order to quantify the dislocation substructures which develop during the plastic straining in temperature. From a predictive point of view, the physical mechanisms as dislocation glide or stress gradient localization across the thickness are studied by numerical simulations using a previously described single crystal strain gradient plasticity model [26]. The evolution of the size effects in fcc materials with temperature will finally be correlated with the corresponding deformation mechanisms (wavy or planar slip character).

2. Experimental procedures and numerical tools

2.1. Material description, samples preparation and microstructural analysis

In this study, three distinct metals were employed: high purity polycrystalline nickel and copper (purity > 99.98 wt%) and polycrystalline Ni-20%wt.Cr. These three metals are used in small mechanical parts in biomedical or electronic devices for instance. The values of the stacking fault energy γ_{sfe} (obtained from literature) of each metal are summarized in Table 1. The slip character of the material is linked to the stacking fault energy through the ratio $\gamma_{sfe} / \mu b^2$ (μ is the shear modulus and b the modulus of the Burger vector of dislocations) which is inversely proportional to the dissociation distance between two dislocations. Cross-slip is then easily activated for materials with large values of $\gamma_{sfe} / \mu b^2$ whereas planar slip metals are characterized by corresponding

low values. The values of this ratio for Ni, Cu and Ni-20%wt.Cr are indicated in Table 1. Cross-slip is then easy for nickel, involving wavy slip character whereas planar slip is dominant for Ni-20wt%.Cr. Copper presents intermediate value of $\gamma_{fe} / \mu b^2$ ensuring deformation mechanisms with cross-slip.

Table 1. For the three materials studied: stacking fault energy γ_{fe}, relative ratio of stacking fault energy $\gamma_{fe} / \mu b^2$ (μ: shear modulus, b: Burgers vector modulus), thickness range of the samples, thickness (t) over grain size (d) ratio corresponding spectrum and references to previous works for more details concerning experimental methods [27, 28].

	γ_{fe} (mJ/m^2)	$\gamma_{fe} / \mu b^2$ (μm^{-1})	Thickness range (μm)	t/d range	Previous works
Nickel	125[(a)]	28.25	12.5 - 3200	1 -12.5	[10]
Copper	45[(a)]	16.4	500	0.9 - 25	[25]
Ni-20wt.%Cr	42[(b)]	8.33	100 - 1600	0.5 - 49	[29]

[(a)] following Meyer and Lewis [27]

[(b)] following Akhtar and Teghtsoonian [28]

Samples consisting of rolled sheets of thickness t ranging from 12.5µm to 3.2 mm were annealed in a secondary vacuum ($P_{O2} < 10^{-5}$ mbar) in order to obtain various grain sizes without oxide layers. Details of the experimental procedures and associated microstructural characterization can be found in previous papers (see for nickel [10], for Ni-20%wt.Cr [29] and for copper [25]). Microstructural observations were performed thanks to conventional metallurgical setups. The grain size distribution of both surface

and cross section was analysed by light microscopy and Scanning Electron Microscopy (SEM). The dislocation substructure of the thermomechanically work hardened samples was observed by TEM with a microscope operating at 200 kV. The thin discs were taken from the middle of the thickness and were prepared using a twin-jet electrolytical thinning apparatus.

Figure 1 represents an overview of the microstructure of the materials. Annealing twin boundaries (Σ_3 type boundaries with coincidence lattice site formalism), which can exist in large fractions for low stacking fault energy materials (Fig. 1(a)) were considered as grain boundaries for the estimation of the average grain diameter [10]. The mean grain size varies in a large spectrum, typically between 20 μm and 571 μm leading to t/d ratios ranging from 0.5 to 50 depending on the material (Table 1). Mean volumetric grain size was computed from all surface grain observations. However, systematic grain observations through the sample thickness were also carried out (Fig. 1(b)). The studied samples got at least one grain through the thickness with generally means a minimum of one free surface per grain. Crystallographic texture analysis was systematically performed by Electron Back Scattered Diffraction (EBSD) using SEM. Schmid factors of each grain (Fig. 1(c)) were registered for all experimental conditions in order to verify the isotropy of the mechanical properties. For a given material, only samples with a similar crystallographic texture were retained in order to avoid any influence of this parameter. The corresponding maximal texture density I expressed in multiples of a random distribution (m.r.d. unit) always takes values lower than five for the three selected materials. Ni-20wt.%Cr alloys can exhibit ordered phases under specific heat treatment conditions [30] but XRD and TEM investigations did not show any presence of such order.

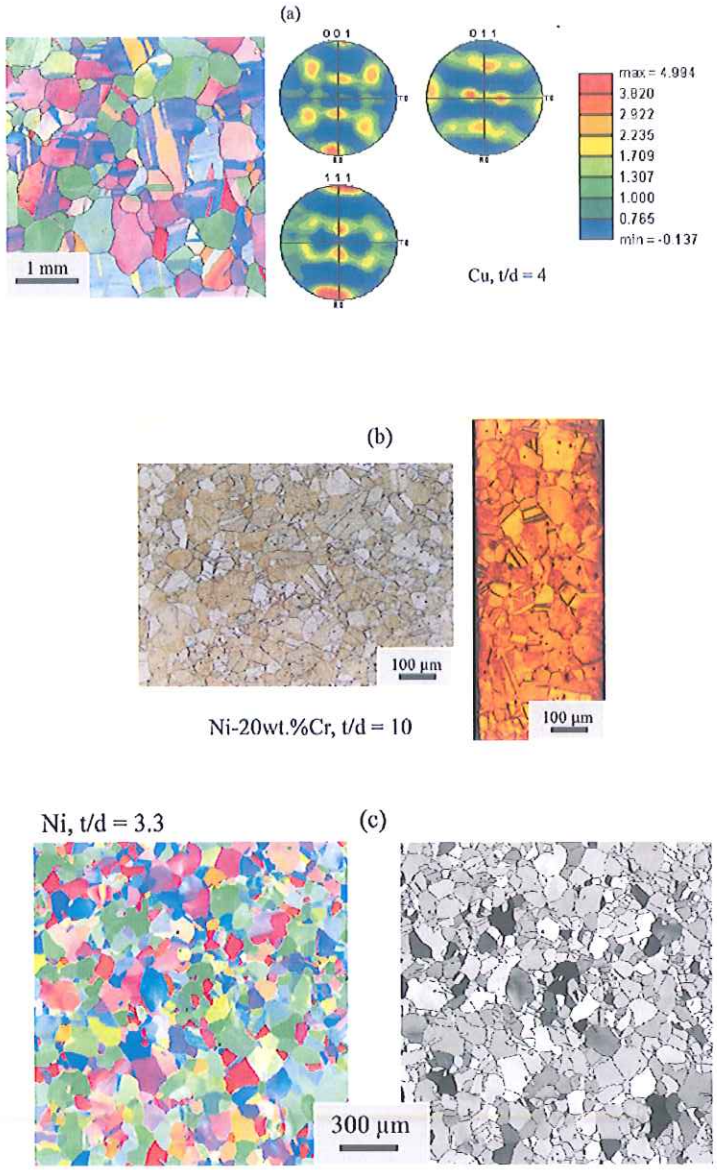

Fig. 1. Microstructures of the materials studied in this work. (a) EBSD grain maps for copper (t/d = 4) showing the existence of twins and corresponding normalized {001}, {011} and {111} pole figures. (b) Ni-20wt.%Cr microstructure on the surface (left) and through the thickness (right) of a t/d = 10 sample. (c) Nickel sample (t/d = 3.3) microstucture, with typical EBSD grain map (in left), and corresponding Schmid factor map (in right) given by a gray scale level in the range 0.273 – 0.5.

2.2. Mechanical testings

To characterize the mechanical behaviour of the three fcc materials, traditional monotonous tensile tests were performed at various temperatures T between 203 K and 1000 K on dog-bone-shaped samples with a gauge section of 20 mm in length and 10 mm in width. Depending on the required resolution, two force cells of 10 kN and 100 N were used. The experiments were strain rate controlled at a strain rate of $2x10^{-4}$ s^{-1}. Lower temperatures were applied to the samples using a climatic room cooled down with liquid nitrogen. Axial deformation was measured by a traditional contact extensometer. High temperature tensile tests were carried out in a three zone furnace and deformation was measured by a contact extensometer with two ceramic extremities.

2.3. Strain gradient crystalline plasticity model

Finite Element Method (FEM) simulations were performed using a single crystal strain gradient plasticity model based on the work of Evers et al [31, 32] and Gurtin [33]. Thanks to the Statistically Stored Dislocations (SSDs) density computed by the model, the single crystal plasticity behaviour can be correctly reproduced. Moreover, the grain size and free surface boundary effect on the mechanical behaviour are correctly modeled by the introduction of the Geometrically Necessary Dislocations (GNDs). This model was correctly identified for nickel at room temperature using single crystalline and polycrystalline experimental tensile curves, and has been successfully employed to investigate size effects in nickel polycrystals [26, 34]. Details about the modeling

strategy, the constitutive law of the model, the mesh and boundary conditions, can be found in a previous paper [26]. To investigate the effect of temperature on the miniaturization size effect, a new identification for Ni was performed. Details of this numerical identification are given in Appendix A. This model can then help to investigate the surface effects occurrence for multi and polycrystals virtually strained at different temperatures.

3. Size effect and temperature in fcc materials: experimental results and strengthening mechanisms

3.1. Temperature effect on the Hall and Petch relation

The grain size dependence of the flow stress s for different strain levels e is well represented by the traditional Hall and Petch (HP) relation [35]:

$$s(e) = s_0(e) + \frac{k(e)}{\sqrt{d}} \quad (1)$$

$s_0(e)$ and $k(e)$ are material empirical constants which depend on strain. Fig. 2(a) shows a typical HP plot for Ni-20wt.%Cr, with a large thickness value, plastically strained at room temperature at a value of 0.098. Two distinct regimes are clearly evidenced separated by the critical ratio $(t/d)_c$. This breakdown in the HP relation has been observed for the three studied material, for various thicknesses, in a more or less pronounced fashion. The first regime (low grain sizes, right part of the graph) is representative of the polycrystalline behaviour and HP parameters (k_P, s_{0P}) are in agreement with literature [36-38]. In the second regime (large grain sizes, left part of the

graph), the dependence on the grain size increases more significantly which leads to a sensitive decrease in stress. This effect strongly modifies the HP coefficients (k_M, σ_{0M}) which characterize the multicrystalline behaviour of the materials [17, 39].

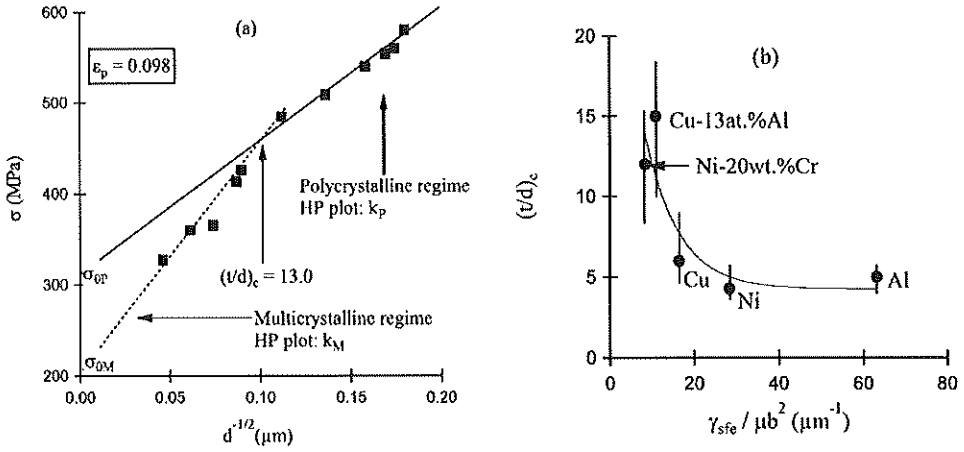

Fig. 2. (a) Typical HP plot at room temperature for Ni-20wt.%Cr alloy with a thickness t = 1.6 mm. Data obtained for ε_p = 0.098 showing the critical ratio $(t/d)_c$ separating the polycrystalline and the multicrystalline regimes. (b) Relationship between $(t/d)_c$ and the relative ratio of stacking fault energy $\gamma_{fe} / \mu b^2$ for different materials and different thickness values. Vertical lines include the different values which can be found in literature. Reference data: Cu [14, 38] and this work; Cu-13at.%Al [14]; Ni [40] and this work; Ni-20wt.%Cr this work; Al [14, 23, 41].

Experimentally, it can be observed that $(t/d)_c$ increases with strain in a more or less pronounced mode. The average value of $(t/d)_c$ strongly depends on the material, ranging around 3-5 for nickel, 5-8 for copper, up to a value of 9-14 for Ni-20wt.%Cr. A direct link is obtained between $(t/d)_c$ and the ratio $\gamma_{fe} / \mu b^2$ as evidenced in Fig. 2(b) which compiles the result of this work with several values issued from the literature. The predominance of planar glide and stacking fault formation (*i.e.* materials with low

values of $g_{fe} / \mu b^2$) leads to a transition from polycrystalline to multicrystalline behaviour for large values of *t/d* ratios compared to easy cross-slip materials (*i.e.* materials with large values of $g_{fe} / \mu b^2$). Moreover, $(t/d)_c$ values for low $g_{fe} / \mu b^2$ materials (especially for solid solution alloys) are more scattered, being strongly thickness dependent.

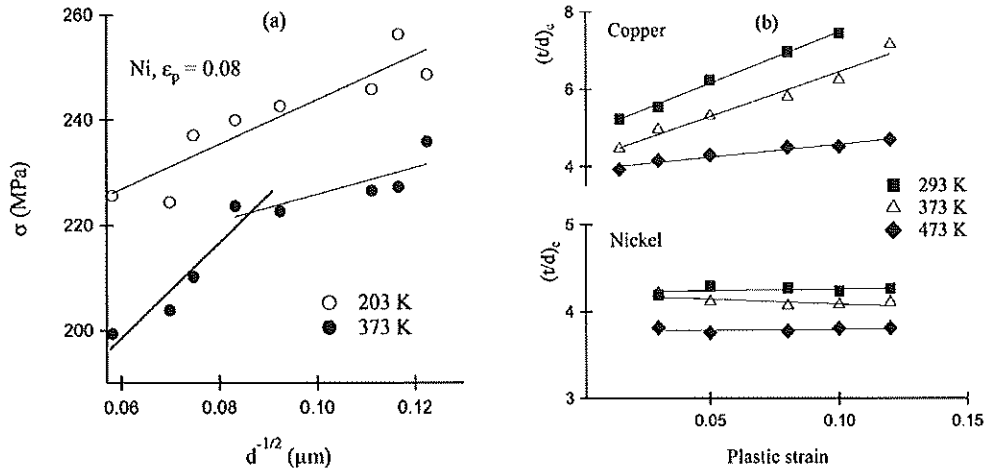

Fig. 3. (a) HP law for nickel at two temperature levels (plastic strain of 0.08). (b) Evolution of the critical ratio $(t/d)_c$ with plastic strain and temperature for copper and nickel.

Experiments performed in frozen conditions (T = 203 K) do not exhibit a transition in the HP law (Fig. 3(a)), independently of the plastic strain level. The HP law is always verified in this temperature contrarily to the results obtained at room temperature. Inversely, the transition between polycrystalline and multicrystalline regimes is always evidenced for temperatures larger than 293 K (Fig. 3(b)). Moreover, the critical ratio $(t/d)_c$ takes lower values as the temperature rises. This temperature effect is more sensitive when $g_{fe} / \mu b^2$ is weak. The critical plastic strain level at which the breakdown

of the HP relation happens seems to be independent of the temperature: around 0.015 for copper and around 0.03 for nickel. As soon as this critical strain level is reached, the evolution of $(t/d)_c$ with the plastic strain level is the same for all temperatures: roughly constant for nickel, and following an increasing linear relationship for copper.

3.2. Strengthening parameters: Kocks-Mecking formalism

Plastic straining mechanisms can be conveniently described in terms of simple models using a single scalar parameter for the description of the dislocation structural features, namely the dislocation density r [42, 43]. Indeed, the strengthening behaviour of fcc materials can be captured by the frequently used one-parameter model developed by Kocks and Mecking [44, 45]. In this model, the work hardening is assumed to be controlled by a competition between the progressive storage of dislocations (predominant during the second hardening stage) and their annihilation (predominant during the third hardening stage) [46]. The average dislocation density r, and its kinetic evolution with plastic strain $dr/d\varepsilon_p$, is the physical internal scalar variable linked with this model. The basic relation of this model takes the following form [43, 47]:

$$dr = \left(\frac{dr}{d\varepsilon_p}\right)^{+} - \left(\frac{dr}{d\varepsilon_p}\right)^{-} \cdot d\varepsilon_p \qquad (2)$$

The dislocation accumulation term $\left(dr/d\varepsilon_p\right)^{+}$ represents the increase in dislocation length per slipped area. For most of the cases, it can be established to be proportional to

$\sqrt{r}$. The annihilation term $\left(dr/d\varepsilon_p\right)^-$ is associated with recovery mechanisms of the dislocation density and is directly proportional to r according to Kocks [44, 46].

The evolution rate of the dislocation density with ε_p can be therefore derived from Eq. (2), assuming the knowledge of the accumulation and annihilation terms. Taking a very wide formalism, initially stated by Mughrabi and Essman [47], and subsequently amended [17, 48, 49], $dr/d\varepsilon_p$ can be written as the sum of four parts:

$$\frac{dr}{d\varepsilon_p} = \frac{M\sqrt{r}}{\delta b} + \frac{Mk_g}{bd} + \frac{M}{bL} - \frac{2MPy}{b} \tag{3}$$

The first component is the traditional accumulation term related to the athermal storage of mobile dislocations. δ means the ratio between the mean free path of mobile dislocations L and the average dislocation distance l :

$$\delta = \frac{L}{l} = L\sqrt{r} \tag{4}$$

The second term takes into account the existence of the GND density linked to the grain boundaries, following the suggestion of Ashby [50]. In this part, k_g is a material constant linked, among other parameters, to the grain shape [46]. This term is predominant at the beginning of the plasticity and can be correlated to the development of intergranular internal stresses inside the polycrystal. The third term is related to the initial dislocation structure which is characterized by a mesh size L. Finally, the fourth term on the right hand side takes into account the contribution of cross-slip mechanisms which progressively take place at higher plastic strain levels [51, 52]. P is the

probability that two dislocations annihilate each other when they are separated by a distance y. This term becomes predominant in the third stage of work hardening.

Furthermore, Eq. (3) can be associated to the traditional Taylor equation (Eq. (5)) linking the flow stress σ to the dislocation density ρ (α is a material parameter relative to the dislocation arrangement and the interaction between slip systems, and M the Taylor factor):

$$\sigma = \alpha M b \sqrt{\rho} \tag{5}$$

This relation holds for fcc crystals plastically strained on a large range of plastic stress under polyslip conditions [53]. Therefore, the general following relationship can be expressed, combining Eqs. (3) and (5) [17]:

$$\sigma\theta = \frac{\alpha M^2}{2b}\sigma + \frac{\alpha^2 M^3 b}{2}\frac{k_g}{d} + \frac{1}{L} - \alpha^2 M^3 b \rho y \tag{6}$$

where $\theta = d\sigma/d\varepsilon$ is the work hardening rate of the material. The plot of $\sigma\theta = f(\sigma)$, so-called Kocks-Mecking plots, can be therefore used to illustrate Eq. (6). Such plots are shown in Fig. 4 for copper at room temperature and for two extreme values of the t/d ratio. Three distinct hardening stages can be identified. A detailed description of each one can be found in traditional reviews [44, 46, 54, 55]. For fcc isotropic polycrystals (no crystallographic texture), the first stage is very weakly pronounced. The second stage is related to the activation of multiple gliding systems and the existence of a few cross slips [51]. In this stage, the linear part of the $\sigma\theta = f(\sigma)$ curve, of slope D_I, defines the second work hardening stage. The last term on the right side of Eq. (6) can be

neglected due to the low probability to develop cross-slip. This equation can therefore be approximated under the following synthetic form for the second hardening stage:

$$\sigma = D_{II}\varepsilon + (\sigma)_0 \tag{7}$$

with:

$$D_{II} = \frac{\alpha\eta M^2}{2b} \tag{8}$$

and:

$$(\sigma)_0 = \frac{\alpha^2\eta^2 M^3 b}{2}\left(k_g\frac{\varepsilon}{d} + \frac{1}{L}\right) \tag{9}$$

D_I is the latent hardening, corresponding to the short-distance interactions between dislocations, for instance interaction between mobile dislocations and Franck network [56]. The grain boundary contribution due to the GNDs and the one related to the initial dislocation structure are taken into account by the $(\sigma)_0$ parameter.

Previous works [17, 18] showed that the main parameters of this formalism can be used to capture the occurrence of size effects on the work-hardening mechanisms at room temperature. In order to analyze more accurately the effect of temperature on such size effects, the next part of this paper deals with the modification of these parameters with temperature and *t/d* ratio.

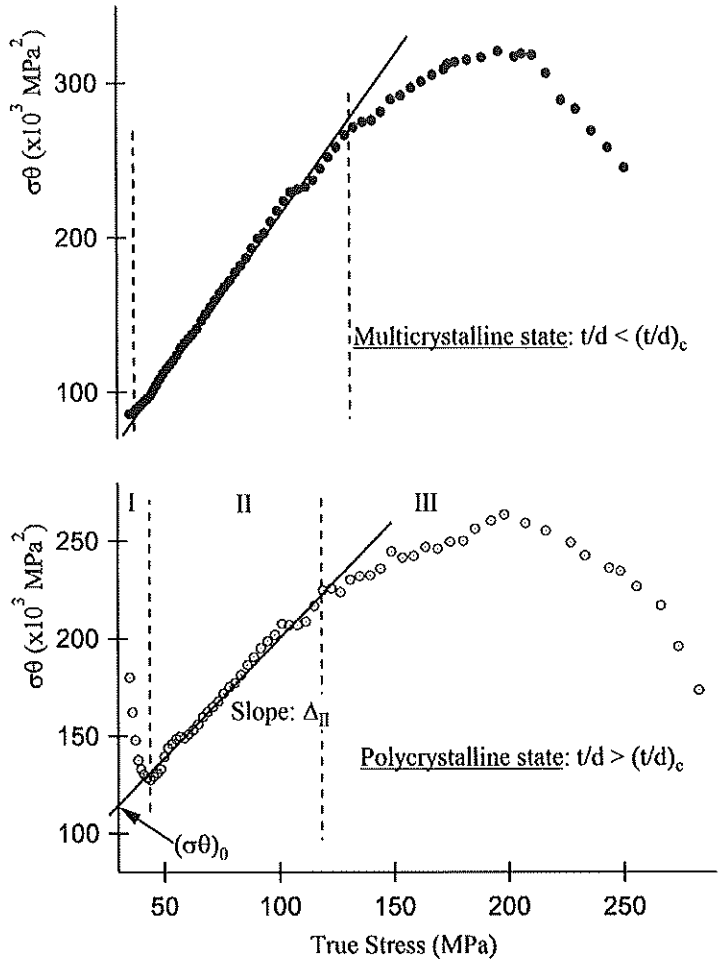

Fig. 4. Examples of $s_q = f(q)$ plots for copper with two extreme values of *t/d* ratio (room temperature).

3.3. Temperature dependence of the size effects on the strengthening mechanisms

The temperature dependence of the strengthening properties has been intensively investigated for fcc metals and alloys, for both single crystals [57, 58] and polycrystals [59-61]. Our results agree with these previous works. For polycrystals and multicrystals, the change in deformation modes with an increase in temperature is closely related to

the thermal activation controlled mechanisms such as cross-slip. As a consequence, the second work hardening stage progressively disappears with the increase in T, independent of the t/d ratio. Hence, the third hardening stage takes place at lower values of plastic strain [25].

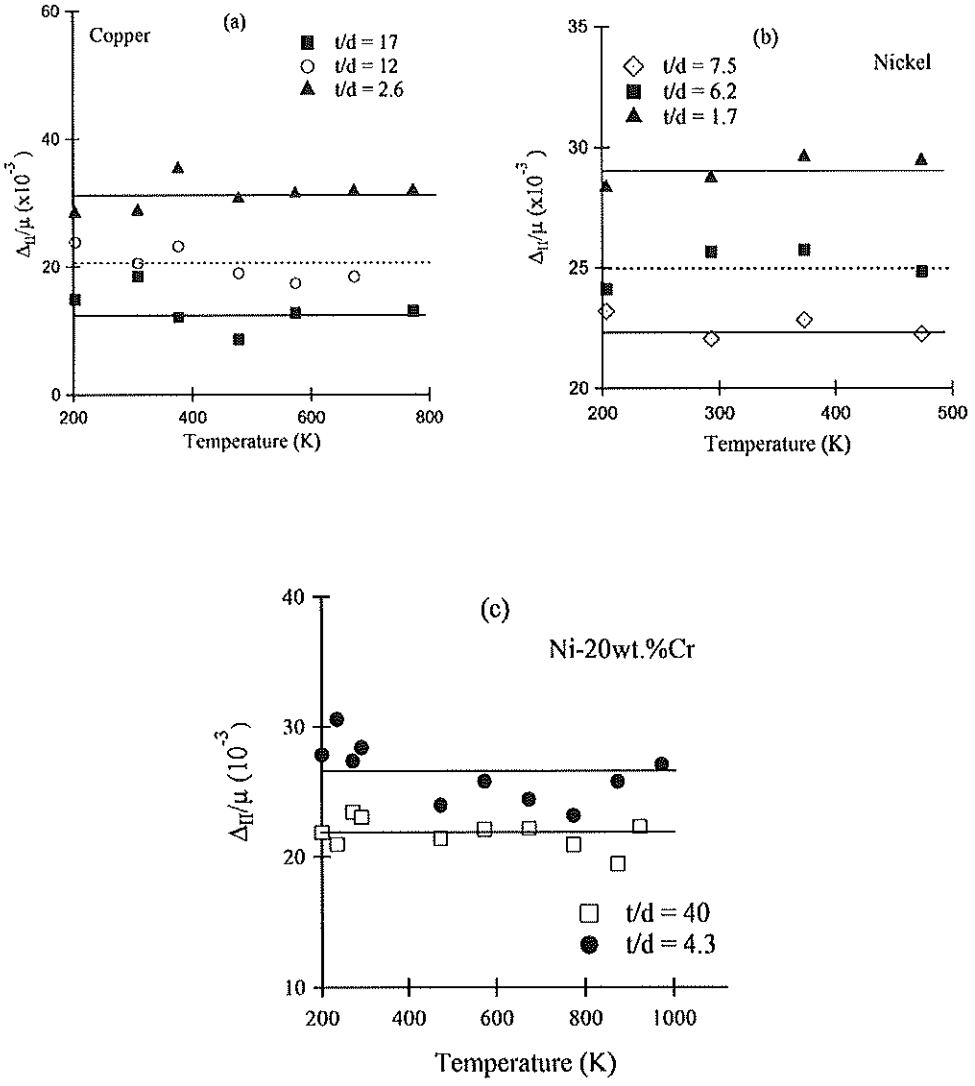

Fig. 5. Evolution of the normalized value of the latent hardening D_I/μ with temperature and t/d ratio. (a) Copper, (b) nickel, (c) Ni-20wt.%Cr.

If normalized by the shear modulus, which temperature dependence follows Eq. (10) [59] (μ_0 and b_0 being empirical constants which can be found in literature [62, 63]):

$$\mu(T) = \mu_0 \exp(-b_0 T) \tag{10}$$

the latent hardening rate D_{II} remains constant independent of T (Fig. 5). Eq. (8) can be rewritten in another convenient form:

$$\frac{D_{II}}{\mu} = \frac{\alpha M^2}{2b} \tag{11}$$

In this equation, the variation of M (no significant variation of texture and Schmid factors for the samples observed by EBSD) and α with temperature is weak for homologous temperatures T/T_f ranging between 0.1 and 0.5 [44]. Therefore b must take a constant value independent of the temperature. So, according to Eq. (4), the mean free path of gliding dislocations L and the average dislocation distance l vary in the same way with temperature during the second hardening stage. Previous TEM analyses evidenced an increase in the mean cell size f with temperature for polycrystals and multicrystals plastically strained at various temperatures [25]. This is in agreement with the similitude concept developed by Kuhlman-Wilsdorf [64] which states a constant relationship between l and f. This feature can be correlated with an increase in both parameters L and l.

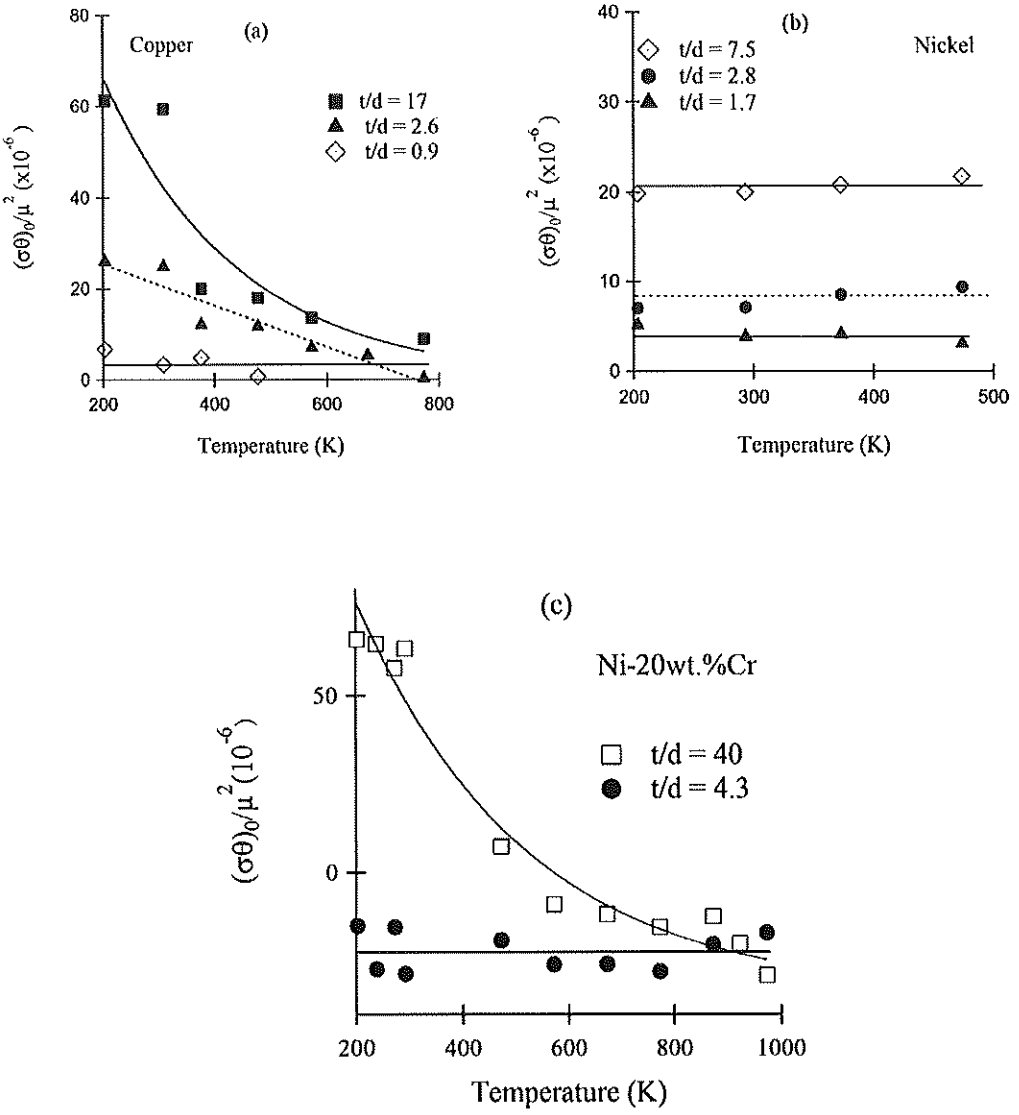

Fig. 6. Evolution of the $(sq)_0/\mu^2$ parameter with temperature and *t/d* ratio. (a) Copper, (b) nickel, (c) Ni-20wt.%Cr.

The parameter $(sq)_0/\mu^2$ strongly decreases with an increase in temperature for polycrystalline specimens of copper (Fig. 6(a)) and Ni-20wt.%Cr (Fig. 6(c)), but remains constant for nickel (Fig. 6(b)). For specimens with $t/d < (t/d)_c$, this parameter

remains constant with temperature for all materials. So, with a decrease in $g_{fe} / \mu b^2$, the difference in $(sq)_0/\mu^2$ between polycrystals and multicrystals tends to be reduced with an increase in temperature.Two distinct phenomena can explain this result. The first one could be linked to a decrease in the dependence on the grain size of $(sq)_0/\mu^2$ for polycrystals. Indeed, the increase in temperature generally induces a decrease in the long range backstress which is linked to the GNDs, due to the early cross-slip activation. The second phenomenon could be related to the role played by free surfaces in polycrystals, which act as potential sinks for dislocations. A competition between both origins is hence possible. In order to disassociate these two mechanisms, a methodology is proposed in the next section, supported by the experimental results concerning temperature effects on the strengthening behaviour of both polycrystalline and multicrystalline materials.

4. Disassociation of the grain size effects and the intrinsic surface effects

In order to disassociate the grain size and surface contributions to work hardening mechanisms, $(sq)_0/\mu^2$ can be expressed by an expanded relationship taking into account the surface effects [25, 45]:

$$\frac{(sq)_0}{m^2} = \frac{a^2 M^3 b}{2} \left(k_g \frac{1}{d} + \frac{1}{L} - \frac{1}{s} \right) \qquad (12)$$

This equation enlarges the relation (9) by adding a supplementary term proportional to *1/s*. This parameter was briefly introduced by the pioneering works of Mecking [45], in order to take into account the contribution of dislocation sinks such as free surfaces

where dislocations can be annihilated. These dislocation sinks are characterized by a positive mesh size *s* which tends to locally decrease the dislocation density.

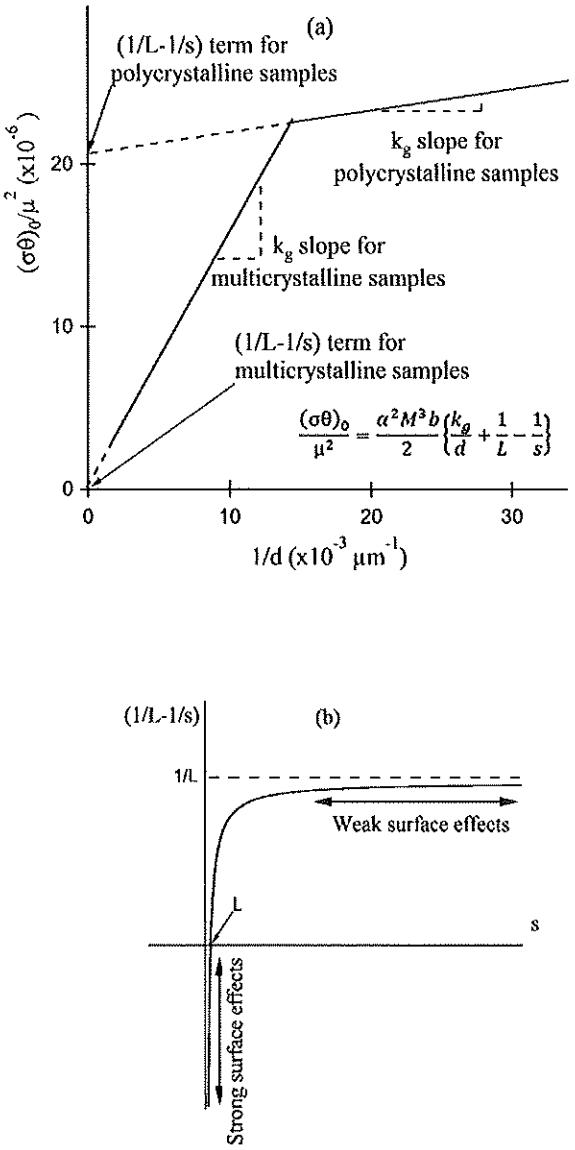

Fig. 7. (a) Typical plot of $(\sigma\theta)_0/\mu^2$ versus *1/d* showing two distinct stages and corresponding parameters (Ni, T = 473 K). (b) Mathematical evolution of *(1/L – 1/s)* with the variable *s*. The areas where the surface effects predominate and are negligible are indicated in this plot.

The contribution of grain boundaries and surface effects on $(\sigma_0)_0/\mu^2$ can be estimated using the experimental results presented in this work. In order to illustrate the grain size dependence of $(\sigma_0)_0/\mu^2$, this parameter can be plotted versus $1/d$ for each temperature level. Such a graph is given in Fig. 7(a) for Ni work hardened at T = 473K. As for HP plots, a strong breakdown in the slope value, representative of the transition between polycrystalline and multicrystalline behaviours, can be observed. So, for each temperature and each state of the samples (*i.e.* multicrystals or polycrystals), it is possible to compute k_g and $(1/L - 1/s)$ following Eq. (12). These two terms characterize respectively the grain size influence and the balance between the contribution of initial dislocation structures ($1/L$) and surface effects ($1/s$).

The first parameter, k_g, is directly linked to the GND density ρ_{GND}, the grain size d and the deformation level ε according to [50]:

$$\rho_{GND} = \frac{M k_g \varepsilon}{b d} \tag{13}$$

At the beginning of the plastic strain process, GNDs bring the main contribution to the work hardening. Combining Eqs (13) and (5) with $\rho \approx \rho_{GND}$ leads to:

$$\sigma = \alpha \eta \mu b^{1/2} M^{3/2} k_g^{1/2} \sqrt{\frac{\varepsilon}{d}} \tag{14}$$

This equation can be directly related to the HP law indicating a proportional relationship between the HP coefficient k and k_g: $k = C\sqrt{k_g}$ with C a material constant for a given

deformation level. Grain size contribution in Eq. (12) can therefore also be analysed in terms of HP constant k.

Fig. 7(b) gives the evolution of *(1/L-1/s)* with s and indicates the schematic location of strong and weak surface effects behaviours. In the following section, the evolution of both parameters with temperature is studied depending on $g_{fe} / \mu b^2$.

4.1. Easy cross-slip fcc metals: the case of nickel

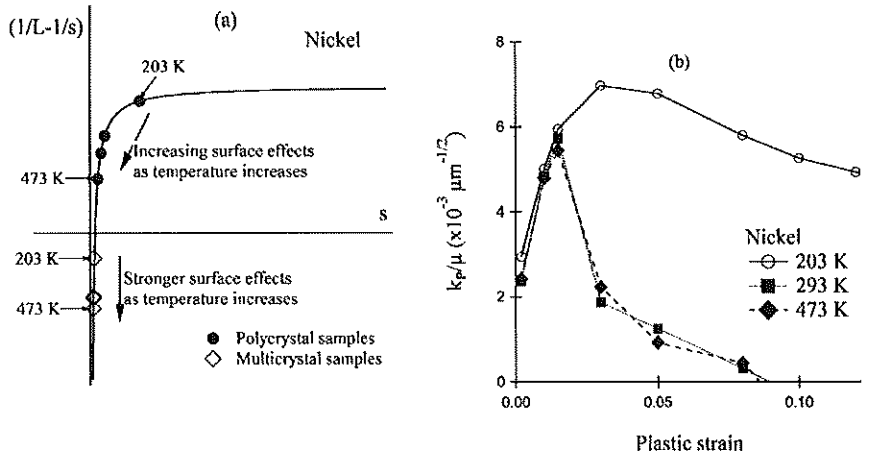

Fig. 8. (a) Schematic location on the *(1/L – 1/s) = f(s)* curve of the various samples of nickel. (b) Evolution for polycrystalline Ni of the Hall-Petch k_P parameter with temperature.

For nickel, the temperature dependence on the work hardening is characterized by a constant value of both D_I/μ and $(sq)_0/\mu^2$ parameters independently of the kind of samples (*i.e.* polycrystalline or multicrystalline states). The application of the disassociation methodology to the experimental results of Fig. 6(b) leads to the synthesis plots given in Fig. 8. Concerning surface effects (Fig. 8(a)), multicrystalline

samples exhibit stronger surface effects when the temperature increases. For polycrystals, when the temperature increases up to 473 K, a decrease of *(1/L – 1/s)* parameter is highlighted which corresponds to surface effects developing inside these samples (the initial mesh size L is considered to be constant due to the same forming processes and heat treatments experienced by the samples). However, *(1/L – 1/s)* is still positive meaning that these surface effects remain moderate. An increase in temperature induces, hence, stronger surface effects for both multi- and polycrystals.

As reported previously, grain size effect remains weak for multicrystals [40]. This effect is found to be independent of the level of temperature. For polycrystals, the grain size contribution on the work hardening mechanisms in temperature has been studied by the evolution of the HP parameter k_P with the plastic strain, for various temperature levels (Fig. 8(b)). For $T = 203$ K, k_P/μ strongly increases in the first work hardening stage and slowly decreases during the second work hardening stage. For higher temperatures, after the same increase of k_P/μ during the first work hardening stage, a very strong decrease in this parameter as a function of the plastic strain is observed. After this strong decrease, the temperature has no longer an effect on this evolution. As a consequence, concerning polycrystals, the stress level in the third hardening stage is weakly dependent on the grain size and this dependence is not influenced by an increase in temperature.

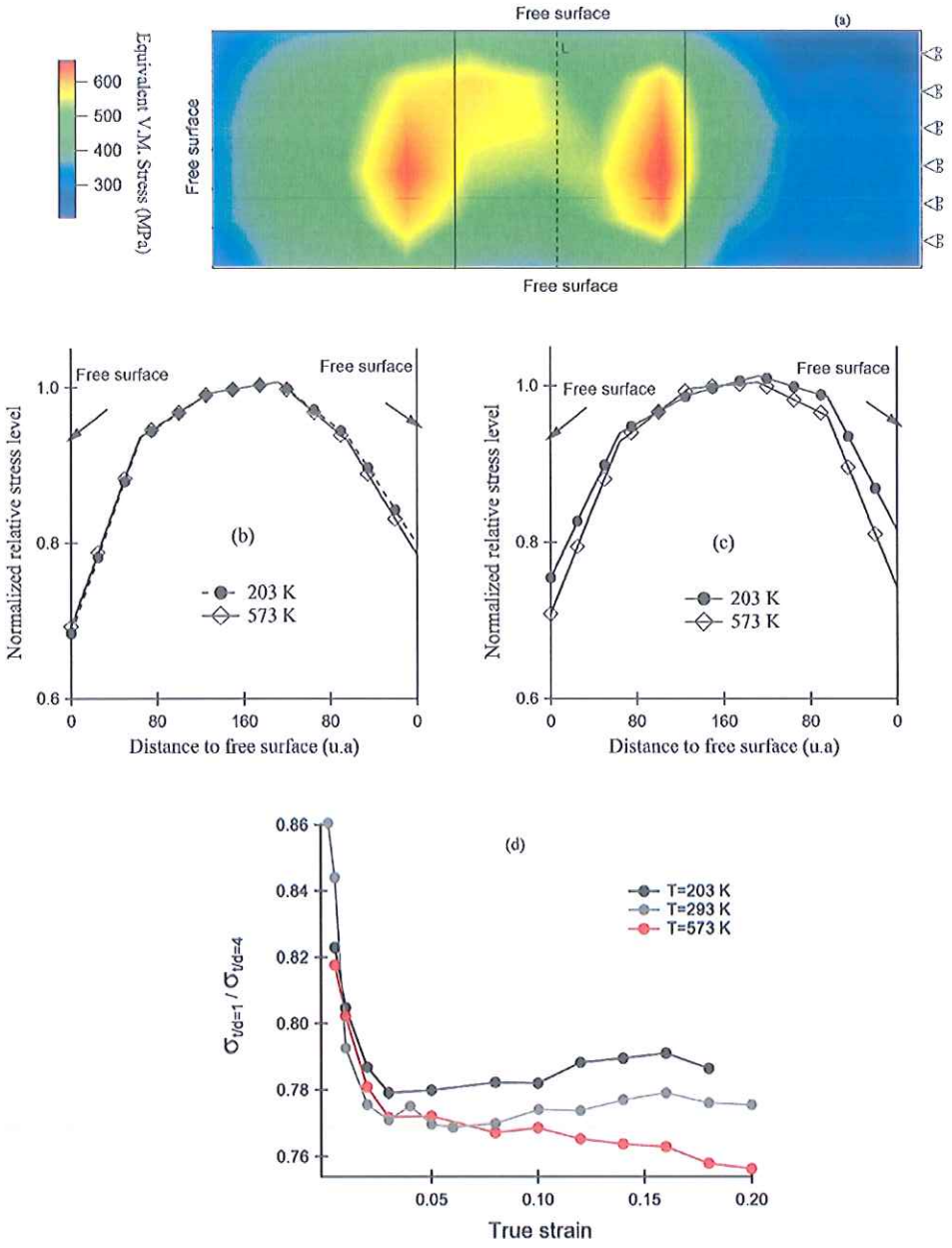

Fig. 9. (a) von Mises equivalent stress distribution in the median cross section of a Ni multicrystalline sample (t/d = 1, ε_p = 0.07) at room temperature. Profiles of the corresponding relative stress level s/s_{center} as a distance to the free surfaces along the line L depicted in Fig. 9(a), and for two temperature conditions: (b) work hardening in stage II, (c) work hardening in stage III. (d) Numerical computation of the ratio between stress levels for multicrystals and polycrystals for various temperature and strain levels.

For easy cross-slip metals (*i.e.* with large values of $g_{fe} / \mu b^2$), surface effects tend therefore to be more pronounced when the temperature increases (for polycrystals and multicrystals). Moreover, as the grain size contribution is weakly dependent on temperature, the difference in mechanical behaviour between the two kinds of samples remains large independently of the temperature. This leads to an almost constant value of $(sg)_0/\mu^2$ independent of the temperature, as observed in Fig. 6(b).

To confirm these results, numerical simulations using the strain gradient crystal plasticity model described above, previously identified for different temperatures (see Annex 1), were carried out. Tensile tests for samples with 1 grain across the thickness (i.e. multicrystal specimens) and 4 grains across the thickness (i.e. polycrystal specimen) were then numerically performed for three different temperatures. In order to compare the mechanical behaviour between multicrystals and polycrystals, the von Mises equivalent (V.M.E) stress distributions were first plotted for the cross sections of the two kinds of samples. Fig 9(a) illustrates the V.M.E stress distribution for a multicrystal strained in stage III (ϵ=0.07) at room temperature. As expected, this distribution is not homogeneous with lower stress values near free surfaces due to surface effects. Figure 9(b) and 9(c) represent the V.M.E stress profiles along the line L depicted in figure 9(a), for multicrystalline samples virtually strained at 203K and 573K, in strain hardening stage II and III, respectively. Theses profiles show stronger stress gradients for larger temperatures in agreement with the experimental results. This increase is nevertheless weak, especially in stage II. For polycrystalline samples, numerical simulations reported the same trend. The corresponding mechanical softening

can be computed as the ratio $s_{t/d=1}/s_{t/d=4}$ between stress levels for multicrystals (t/d = 1) and polycrystals (t/d = 4) for different strain levels. The evolution of such a ratio, illustrated Fig. 9(d), shows a weak increase (less than 4% between the lower and larger value of temperature). As the grain size effect is weak for nickel and is no longer effective for large temperature, this slight increase in softening suggests that surface effects are slightly stronger for polycrystals but not enough to induce a modification of the overall mechanical behaviour between the two kinds of samples.

As a consequence, for wavy slip metals such as nickel, a moderate increase in temperature does not reduce the softening of the mechanical behaviour due to miniaturization.

4.2. Effect of a decrease in $g_{fe} / \mu b^2$: the case of copper and Ni-20wt.%Cr

The values of $(1/L - 1/s)$ are given in Fig. 10(a) for each type of samples and temperatures concerning copper. As shown in this figure, the difference between polycrystals and multicrystals is significantly enhanced with an increase in temperature. In polycrystals, mechanisms are driven by a strong decrease in the surface effects as the temperature rises, whereas the strong surface effects, already present at room temperature for multicrystal samples, persist with substantially identical amplitude for any temperature value.

The evolution with temperature of the HP slopes k_P of the polycrystalline state is given in Fig. 10(b). The corresponding slopes k_g, normalized by the values k_{g203} obtained at the lowest temperature (203 K) are given in Fig. 10(c). The ratio k_g/k_{g203} and the HP

parameter k_P decrease with temperature for copper, in a more sensitive way for polycrystals than for multicrystals. The contribution of grain boundaries to the strain hardening mechanisms in the second hardening stage progressively vanishes with temperature for both kinds of samples. This behaviour is clearly opposite to the one observed for nickel samples.

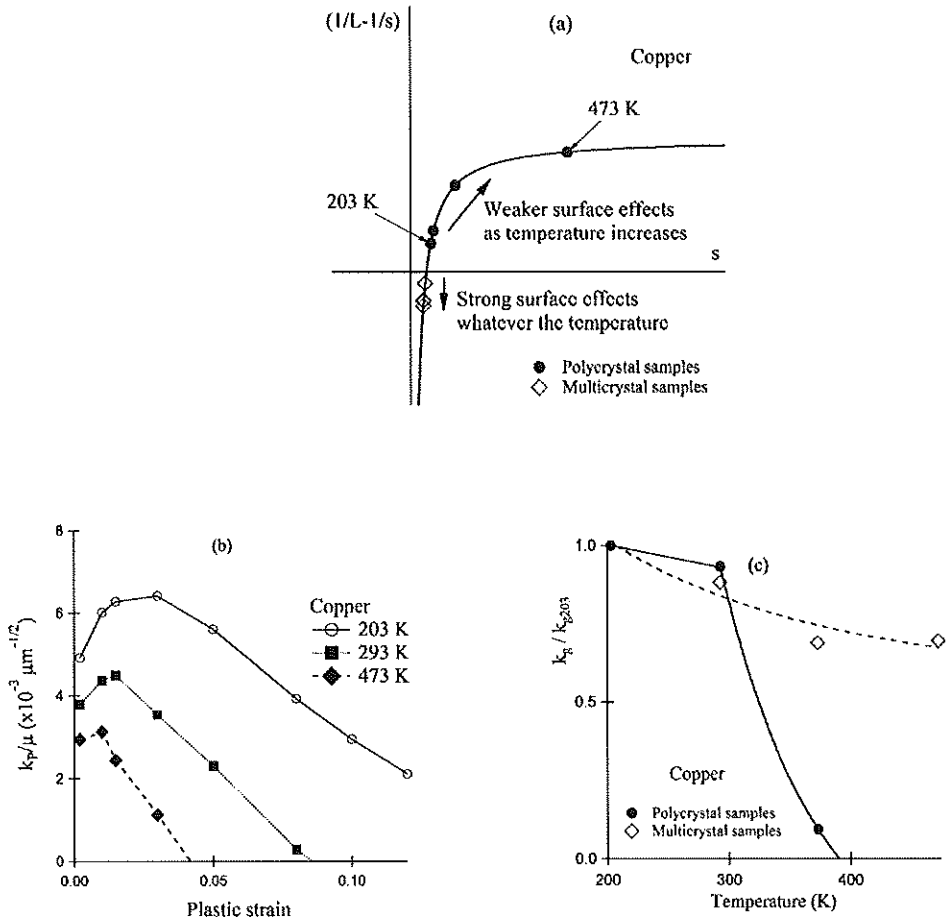

Fig. 10. (a) Schematic location on the *(1/L – 1/s) = f(s)* curve of the various samples of copper. (b) Evolution for polycrystalline Cu of the Hall-Petch k_P parameter with the temperature. (c) Relative evolution for copper of the k_g parameter with temperature representing the grain size effect. Results are given for polycrystal and multicrystal samples.

The decrease in $(sq)_0/\mu^2$ with the temperature for copper polycrystals shown in Fig. 6(a) is then a softening effect directly linked to the weaker influence of the grain boundaries on the strengthening mechanisms. This softening effect is linked to the generalization of cross-slip and the corresponding predominance of the third work hardening stage. For copper samples with low *t/d* values, the strong surface effects developed at low temperatures persist at higher temperatures. This mechanism is accompanied by a slight decrease in the influence of the grain boundaries. Polycrystal behaviour therefore tends to be toward that of multicrystal as the temperature increases.

Dislocation cell observations in copper during the various work hardening stages support this softening mechanism. TEM analyses of the cell structure were performed on samples with low and high *t/d* ratios in the temperature range of this work. Specimens were strain hardened in the second and third hardening stages before observations and the mean cell diameter was computed using a statistical methodology described in detail elsewhere [19]. Results of these observations are given in Fig. 11 in a synthetic way. Dislocation cell sizes in the second hardening stage remain constant, independent of the temperature, for both polycrystalline and multicrystalline samples. Moreover, the increase in cell diameter from polycrystal toward multicrystal is maintained independent of the temperature level. This feature is related to the independence of the latent hardening rate with temperature. When samples are strain hardened in the third stage, mean cell diameter of both sample states are sensitively different at the lower temperature levels. As the temperature increases, the cell size tends towards the same values. So, the mechanical behaviour of polycrystalline samples

tends to be that of multicrystalline ones in copper due to a grain size softening effect which level the mean dislocation cell dimensions between polycrystalline and multicrystalline samples.

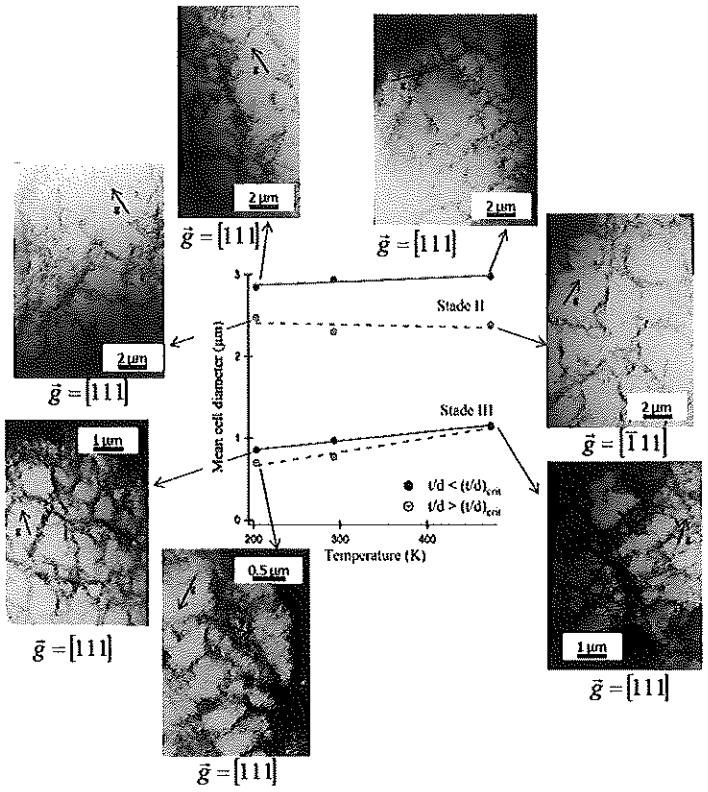

Fig. 11. Dislocation cell structures in copper polycrystal and multicrystal strained in second and third hardening stages. Evolution of the corresponding mean cell diameter with temperature.

Finally, there is indeed a very similar behaviour of copper and Ni-20wt.%Cr alloy concerning the $(\varepsilon\dot{\varepsilon})_0/\mu^2$ parameter (Figs. 6(a) and 6(c)) despite a strong difference in dislocation structures for both materials.

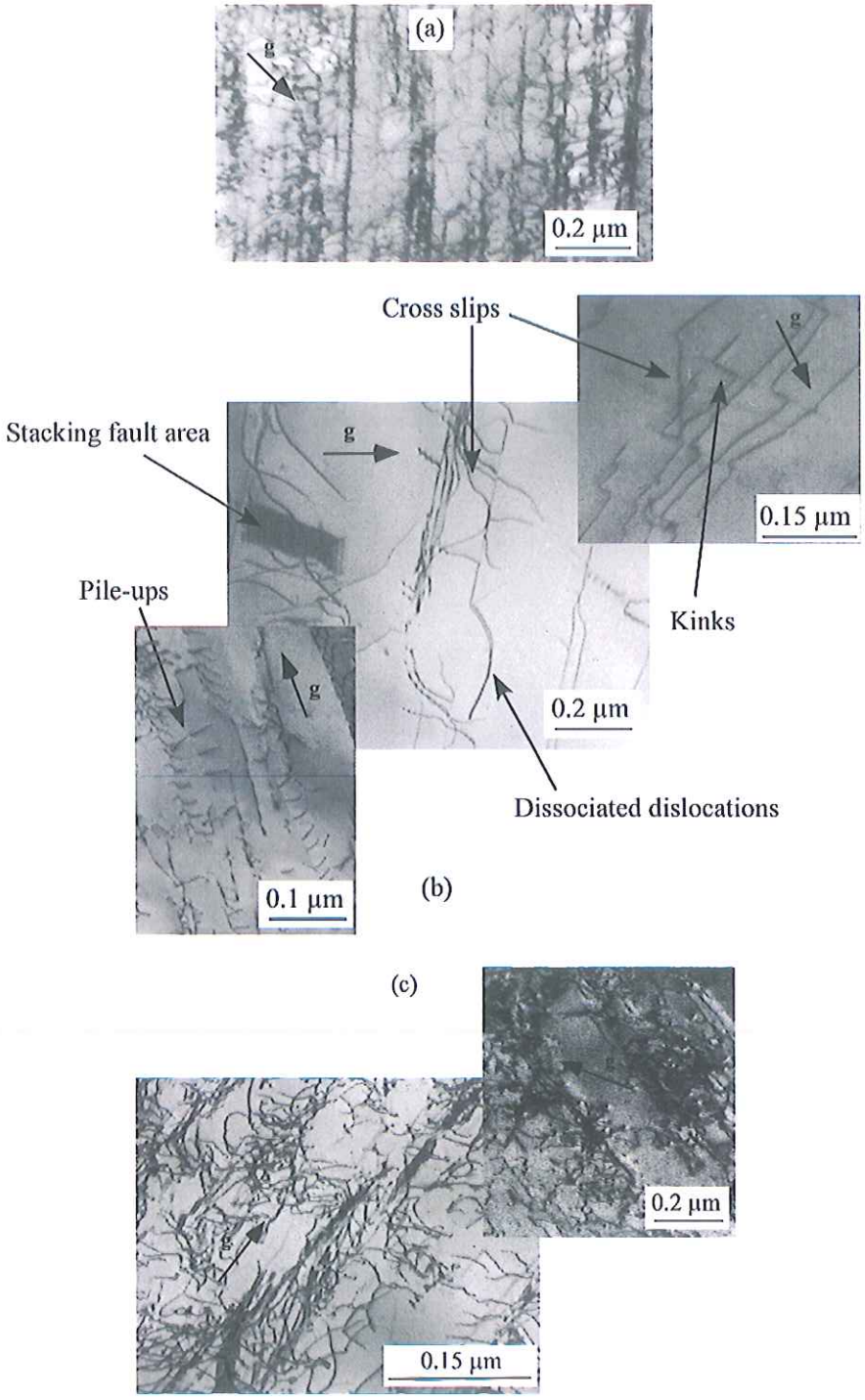

Fig. 12. Dislocation substructures observed in Ni-20wt.%Cr alloys. (a) $t/d > (t/d)_c$, stage II ; (b) $t/d < (t/d)_c$, stage II ; (c) $t/d < (t/d)_c$, stage III (room temperature).

Alloying nickel by chromium decreases the relative stacking fault energy $\gamma_{fe} / \mu b^2$ (Table 1) below a magnitude in which no cell structure is formed [65]. This enhances the formation, in stage II of work hardening, of dislocation blocks separated by geometrically necessary boundaries [66, 67] (Fig. 12(a)). These dislocation substructures have already been observed by Dudova *et al* [68].

When *t/d* ratio stands below the critical value (Fig. 12(b)), as for copper and nickel, the second working stage is expanded in detriment of the third one. Dislocation walls are less dense and dislocations tend to remain straight on their slip planes, minimizing their potential energy. Kinks, pile-ups, disassociated dislocations and stacking fault areas are frequently observed. The anisotropic structure widely depicted in the second stage of work hardening for polycrystals is delayed toward the beginning of third stage in multicrystals (Fig. 12(c)). These dislocation substructures, sensitively different from those observed in copper, have no distinct influence on size effect mechanisms in temperature concerning low stacking fault energy materials.

In summary, whatever the dislocation configuration and evolution, the size effect for fcc metals with lower $\gamma_{fe} / \mu b^2$ values seems to be driven by the same physical processes. For these materials, the multicrystals adopt at low temperatures, especially at room temperature, a behaviour similar to that of polycrystals deformed at higher temperatures. However, the behaviour of polycrystals for temperatures larger than room temperature is due to the progressive activation of cross-slip, coupled with a weaker effect of the grain boundaries. Instead, multicrystals behaviour is linked to the strong surface effects generating a significant stress gradient in the thickness of the samples.

5. Conclusion

New experimental results are given in this work concerning the temperature effect on HP behaviour and strain hardening of polycrystalline fcc materials with various *t/d* ratios. The modifications of the work hardening behaviour are strongly dependent of the wavy slip character of the material. With the help of the quantitative investigation of the dislocation structures achieved by TEM observations and numerical analysis concerning the stress gradient across the thickness of samples, the main results can be summarized by the following points:

- ∑ The strengthening properties of polycrystals and multicrystals are dependent on temperature. This behaviour is linked to $g_{fe} / \mu b^2$ but is roughly independent on the dislocation substructure and its evolution with plastic strain.
- ∑ The latent hardening rate keeps a constant value independent of the temperature, respecting the well-known athermal character of the second work hardening stage. In all cases, the value of this parameter is significantly higher for weaker *t/d* ratios.
- ∑ The characteristics of the multicrystalline behaviour are not deeply affected by an increase in temperature, independently of $g_{fe} / \mu b^2$.
- ∑ For easy cross-slip metals such as nickel, an increase in temperature enhances the surface effects for both polycrystals and multicrystals. As a consequence, the macroscopic softening of the mechanical behaviour between polycrystals and multicrystals is only weakly affected by the temperature. For these materials, the

grain size contribution on the mechanical hardening is weak, in particular for high temperatures.

- ∑ With a decrease in $\gamma_{fe} / \mu b^2$ (*i.e.* transition from wavy slip to planar slip mechanisms), an increase in temperature strongly reduces the differences between polycrystals and multicrystals. For these materials, the grain size influence is strongly dependent on temperature. Indeed, as cross-slip activation is restricted by the low value of $\gamma_{fe} / \mu b^2$, cross-slip becomes strongly dependent on temperature contrary to large $\gamma_{fe} / \mu b^2$ materials for which cross-slip is easy independently of T. As a consequence, for polycrystals, an increase in temperature reduces the grain boundaries contribution involving a strong softening of the mechanical behaviour. For multicrystals, the grain strengthening is weak and the mechanical response does not depend on temperature. With an increase in temperature, polycrystal behaviour tends to lean toward that of the multicrystalline one, in turn reducing the microstructural size effects.

In order to take into account the size effects in formability operations of micro-sized components, using appropriate strain paths minimizing the stress gradients inside the metal parts seems to be the most efficient way [3, 6, 69, 70]. This may be accompanied by a suitable choice of the forming temperature but this parameter appears to be second order for multicrystalline specimens.

Appendix A. Numerical identification of the constitutive law for nickel taking into account the effect of temperature

Assuming that the dislocation storage mechanisms are not temperature dependent (athermal storage), the temperature only affects the slip kinetics of each glide system and the recovery mechanisms (cross-slip and climb of dislocation are thermally activated). The temperature influence on the glide kinetics is directly taken into account in the model whereas the effect of temperature on the recovery mechanisms must be introduced by different values of dislocation annihilation distance y (see [26] and previous Eq. (3) in the section 3.2 for the physical meaning of this parameter).

Fig. A1 represents the experimental and predicted tensile curves for nickel samples with four grains across the thickness (with a grain size around 100 μm) for two temperatures: 203 K and 573 K. A good agreement is observed between the experimental tensile curves and those predicted by the model. Table A1 summarizes the value of the annihilation distance for 203 K, 293 K and 573 K. An increase in temperature involves an increase in this parameter in agreement with its thermally activated character.

Table A1. Numerical values of the annihilation distance y between two dislocations for nickel and three temperature levels. y is defined in Eq. (6) and is given in multiple of Burgers vector modulus b (b = 0.25 nm for nickel).

T (K)	203	273	523
y	$4b$	$5.6b$	$9b$

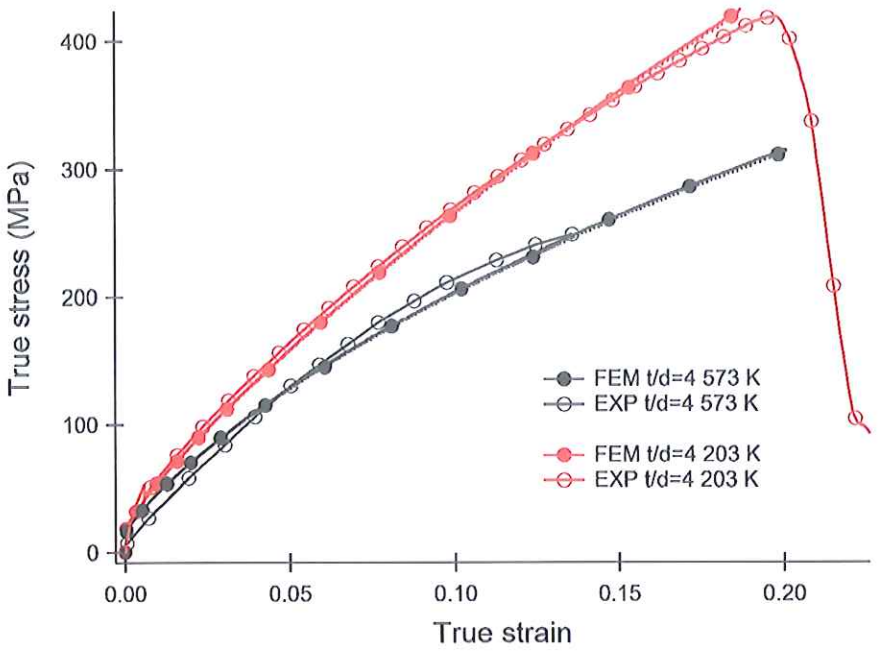

Fig. A1. Comparison between experimental and numerical predicted tensile curves for nickel samples (t/d = 4) and two temperatures: 203 K and 573 K.

Acknowledgements

FNRS – F.R.S. is thanked by A.M. Habraken for financial support. BELSPO through IAP 7.21 research project provides help to A.M. Habraken and L. Duchêne.

References

[1] M.W. Fu, W.L. Chan, Micro-scaled products development via microforming. Deformation behaviours, processes, tooling and its realization, Springer-Verlag, London, 2014.
[2] P.J.M. Janssen, J.P.M. Hoefnagels, T.H. de Keijser, M.G.D. Geers, J. Mech.Phys. Sol., 56 (2008) 2687-2706.
[3] M.W. Fu, B. Yang, W.L. Chan, J. Mat. Proc. Techn., 213 (2013) 101-110.
[4] X. Lai, L. Peng, P. Hu, S. Lan, J. Ni, Comput. Mater. Sci., 43 (2008) 1003-1009.
[5] M. Geiger, M. Kleiner, R. Eckstein, N. Tiesler, U. Engel, CIRP Annals - Manufacturing Technology, 50 (2001) 445-462.

[6] A. Molotnikov, R. Lapovok, C.F. Gu, C.H.J. Davies, Y. Estrin, Mater. Sci. Eng. A, 550 (2012) 312-319.
[7] M.W. Fu, W.L. Chan, Int. J. Adv. Manufact. Techn., (2012) 1-27.
[8] H.-H. Fu, D.J. Benson, M.A. Meyers, Acta Mater., 49 (2001) 2567-2582.
[9] P.J.M. Janssen, T.H. de Keijser, M.G.D. Geers, Mater. Sci. Eng. A, 419 (2006) 238-248.
[10] C. Keller, E. Hug, D. Chateigner, Mater. Sci. Eng. A, 500 (2009) 207-215.
[11] B. Weiss, V. Groger, G. Khatibi, A. Kotas, P. Zimprich, R. Stickler, B. Zagar, Sens. Actuators A, 99 (2002) 172-182.
[12] B. Yang, C. Motz, M. Rester, G. Dehm, Phil. Mag. A, 92 (2012) 3243-3256.
[13] M. Klein, A. Hadrboletz, B. Weiss, G. Khatibi, Mater. Sci. Eng. A, 319-321 (2001) 924-928.
[14] S. Miyazaki, K. Shibata, H. Fujita, Acta Metall., 27 (1979) 855-862.
[15] G. Simons, C. Weippert, J. Dual, J. Villain, Mater. Sci. Eng. A, A416 (2006) 290-299.
[16] S. Geißdörfer, U. Engel, M. Geiger, Int. J. Mach. Tools. Manufact., 46 (2006) 1222-1226.
[17] C. Keller, E. Hug, X. Feaugas, Int. J. Plast., 27 (2011) 635-654.
[18] E. Hug, C. Keller, Metall. Mater. Trans. A, 41 (2010) 2498-2506.
[19] C. Keller, E. Hug, R. Retoux, X. Feaugas, Mech. Mater., 42 (2010) 44-54.
[20] J.-T. Gau, P.-H. Chen, H. Gu, R.-S. Lee, J. Mat. Proc. Techn., 213 (2013) 376-382.
[21] J.-T. Gau, C. Principe, J. Wang, J. Mat. Proc. Techn., 184 (2007) 42-46.
[22] X.L. Geng, B. Wang, Y.J. Zhang, J.X. Huang, M.M. Duan, K.S. Zhang, J. Mat. Proc. Techn., 213 (2013) 574-580.
[23] L.V. Raulea, A.M. Goijaerts, L.E. Govaert, F.P.T. Baaijens, J. Mat. Proc. Techn., 115 (2001) 44-48.
[24] B. Eichenhueller, E. Egerer, U. Engel, Int. J. Adv. Manufact. Techn., 33 (2007) 119-124.
[25] E. Hug, P.A. Dubos, C. Keller, Mater. Sci. Eng. A, 574 (2013) 253-261.
[26] C. Keller, E. Hug, A.M. Habraken, L. Duchene, Int. J. Plast., 29 (2012) 155-172.
[27] R. Meyer, L.J. Lewis, Phys. Rev. B, 66 (2002) 0521061- 0521064.
[28] A. Akhtar, E. Teghtsoonian, Metall. Trans., 2 (1971) 2757-2763.
[29] M. Rudloff, M. Risbet, C. Keller, E. Hug, Mater. Letters, 62 (2008) 3591-3593.
[30] A. Marucco, Mater. Sci. Eng. A, 189 (1994) 267-276.
[31] L.P. Evers, W.A.M. Brekelmans, M.G.D. Geers, J. Mech.Phys. Sol., 52 (2004) 2379-2401.
[32] L.P. Evers, W.A.M. Brekelmans, M.G.D. Geers, Int. J. Sol. Struct., 41 (2004) 5209-5230.
[33] M.E. Gurtin, J. Mech.Phys. Sol., 50 (2002) 5-32.
[34] C. Keller, A.M. Habraken, L. Duchene, Mater. Sci. Eng. A, 550 (2012) 342-349.
[35] A.W. Thompson, M.I. Baskes, W.F. Flanagan, Acta Metall., 21 (1973) 1017-10128.
[36] R.W. Armstrong, J. Mech.Phys. Sol., 9 (1961) 196-199.
[37] S. Nagarjuna, J.T. Evans, Mater. Sci. Eng. A, 466 (2007) 68-70.
[38] T. Tabata, K. Takagi, H. Fujita, Trans. Jap. Inst. Metals, 16 (1975) 569-579.
[39] A.W. Thompson, Scripta Metall., 8 (1973) 145-148.
[40] C. Keller, E. Hug, Mater. Letters, 62 (2008) 1718-1720.
[41] N. Hansen, Acta Metall., 25 (1977) 863-869.
[42] A.S. Argon, Mechanical properties of single-phase crystalline media: deformation at low temperatures, in: P.H. R.W. Cahn (Ed.) Physical Metallurgy, North Holland Elsevier Science BV, Amsterdam, 1996, pp. 1877-1955.
[43] W. Blum, High-temperature deformation and creep of crystalline solids, in: H. Mughrabi (Ed.) Plastic deformation and fracture of materials, VCH Verlagsgesellschaft mbH, VCH Publishers Inc., Weinheim, New York, 1993, pp. 359-405.
[44] U.F. Kocks, H. Mecking, Prog. Mater. Sci., 48 (2003) 171-273.
[45] H. Mecking, Description of hardening curves of fcc single and polycrystals, in: A.W. Thompson (Ed.) Work hardening in tension and fatigue, TMS-AIME, New-York, 1977, pp. 67-88.
[46] J. Gil Sevillano, Flow stress and work hardening, in: H. Mughrabi (Ed.) Plastic deformation and fracture of materials, VCH Verlagsgesellschaft mbH, VCH Publishers Inc., Weinheim, New York, 1993, pp. 19-88.
[47] U. Essmann, H. Mughrabi, Phil. Mag. A, 40 (1979) 731-756.
[48] H. Mecking, U.F. Kocks, Acta Metall., 29 (1981) 1865-1875.
[49] T. Narutani, J. Takamura, Acta Metall., 39 (1991) 2037-2049.
[50] M. Ashby, Phil. Mag. A, 21 (1970) 399-424.
[51] X. Feaugas, Acta Mater., 47 (1999) 3617-3632.
[52] L. Kubin, T. Hoc, B. Devincre, Acta Mater., 57 (2009) 2567-2575.

[53] S.J. Basinski, Z.S. Basinski, Plastic deformation and Work Hardening, in: F.R.N. Nabarro (Ed.) Dislocations in Solids, North-Holland Publishing Company, Amsterdam, 1979, pp. 261-362.
[54] J. Gil Sevillano, I. Ocaña Arizcorreta, L.P. Kubin, Mater. Sci. Eng. A, 309-310 (2001) 393-405.
[55] E. Nes, Prog. Mater. Sci., 41 (1997) 129-193.
[56] J.P. Hirth, Dislocations, in: R.W. Cahn, P. Haasen (Eds.) Physical metallurgy, Elsevier Science Publishers, Amsterdam, 1992, pp. 1223-1258.
[57] M.A. Adams, A.H. Cottrell, Phil. Mag. A, 46 (1955) 1187-1193.
[58] A.H. Cottrell, F.R.S. Stokes, R.J. Stokes, Proc.Roy.Soc.A, 233 (1955) 17-34.
[59] M.-C. Cai, L.-S. Niu, X.-F. Ma, H.-J. Shi, Mech. Mater., 42 (2010) 774-781.
[60] S.R. Chen, U.F. Kocks, High-temperature plasticity in copper polycrystals, in: A.F.a.K. Walker (Ed.) High temperature constitutive modeling, Am. Soc. Mech. Eng., New-York, 1991, pp. 1-13.
[61] N. Gurao, R. Kapoor, S. Suwas, Metall. Mater. Trans. A, 41 (2010) 2794-2804.
[62] L. Rémy, A. Pineau, B. Thomas, Mater. Sci. Eng. A, 36 (1978) 47-63.
[63] Y.P. Varshni, Phys. Rev. B, 2 (1970) 3952-3957.
[64] D. Kuhlmann-Wilsdorf, Mater. Sci. Eng. A, 113 (1989) 1-41.
[65] P.R. Swann, Dislocation arrangements in face-centered cubic metals and alloys, in: J.W. G. Thomas (Ed.) Electron microscopy and strength of crystals, Interscience Publishers, New-York, 1963, pp. 131-181.
[66] X. Feaugas, H. Haddou, Phil. Mag. A, 87 (2007) 989-1018.
[67] N. Hansen, X. Huang, Acta Mater., 46 (1998) 1827-1836.
[68] N. Dudova, R. Kaibyshev, V. Valitov, The Phys. Metals Metall., 107 (2009) 409-418.
[69] P.A. Dubos, E. Hug, M.B. Bettaieb, C. Keller, Metall. Mater. Trans. A, 44 (2013) 5478-5487.
[70] P.A. Dubos, E. Hug, S. Thibault, A. Gueydan, C. Keller, Int. J. Mater. Prod. Technol., 47 (2013) 3-11.

Table captions

Table 1. For the three materials studied: stacking fault energy g_{fe}, relative ratio of stacking fault energy $g_{fe} / \mu b^2$ (μ: shear modulus, b: Burgers vector modulus), thickness range of the samples, thickness (t) over grain size (d) ratio corresponding spectrum and references to previous works for more details concerning experimental methods [27, 28].

Table A1. Numerical values of the annihilation distance y between two dislocations for nickel and three temperature levels. y is defined in Eq. (6) and is given in multiple of Burgers vector modulus b (b = 0.25 nm for nickel).

Figure captions

Fig. 1. Microstructures of the materials studied in this work. (a) EBSD grain maps for copper (t/d = 4) showing the existence of twins and corresponding normalized {001}, {011} and {111} pole figures. (b) Ni-20wt.%Cr microstructure on the surface (left) and through the thickness (right) of a t/d = 10 sample. (c) Nickel sample (t/d = 3.3) microstucture, with typical EBSD grain map (in left), and corresponding Schmid factor map (in right) given by a gray scale level in the range 0.273 – 0.5.

Fig. 2. (a) Typical HP plot at room temperature for Ni-20wt.%Cr alloy with a thickness t = 1.6 mm. Data obtained for ε_p = 0.098 showing the critical ratio $(t/d)_c$ separating the polycrystalline and the multicrystalline regimes. (b) Relationship between $(t/d)_c$ and the relative ratio of stacking fault energy $\gamma_{sfe} / \mu b^2$ for different materials and different thickness values. Vertical lines include the different values which can be found in literature. Reference data: Cu [14, 38] and this work; Cu-13at.%Al [14]; Ni [40] and this work; Ni-20wt.%Cr this work; Al [14, 23, 41].

Fig. 3. (a) HP law for nickel at two temperature levels (plastic strain of 0.08). (b) Evolution of the critical ratio $(t/d)_c$ with plastic strain and temperature for copper and nickel.

Fig. 4. Examples of $\sigma = f(\varepsilon_p)$ plots for copper with two extreme values of t/d ratio (room temperature).

Fig. 5. Evolution of the normalized value of the latent hardening D_{II}/μ with temperature and *t/d* ratio. (a) Copper, (b) nickel, (c) Ni-20wt.%Cr.

Fig. 6. Evolution of the $(s\varrho)_0/\mu^2$ parameter with temperature and *t/d* ratio. (a) Copper, (b) nickel, (c) Ni-20wt.%Cr.

Fig. 7. (a) Typical plot of $(s\varrho)_0/\mu^2$ versus *1/d* showing two distinct stages and corresponding parameters (Ni, T = 473 K). (b) Mathematical evolution of *(1/L – 1/s)* with the variable *s*. The areas where the surface effects predominate and are negligible are indicated in this plot.

Fig. 8. (a) Schematic location on the *(1/L – 1/s) = f(s)* curve of the various samples of nickel. (b) Evolution for polycrystalline Ni of the Hall-Petch k_P parameter with temperature.

Fig. 9. (a) von Mises equivalent stress distribution in the median cross section of a Ni multicrystalline sample (*t/d* = 1, ε_p = 0.07) at room temperature. Profiles of the corresponding relative stress level s/s_{center} as a distance to the free surfaces along the line L depicted in Fig. 9(a), and for two temperature conditions: (b) work hardening in stage II, (c) work hardening in stage III. (d) Numerical computation of the ratio between stress levels for multicrystals and polycrystals for various temperature and strain levels.

Fig. 10. (a) Schematic location on the *(1/L – 1/s) = f(s)* curve of the various samples of copper. (b) Evolution for polycrystalline Cu of the Hall-Petch k_P parameter with the

temperature. (c) Relative evolution for copper of the k_g parameter with temperature representing the grain size effect. Results are given for polycrystal and multicrystal samples.

Fig. 11. Dislocation cell structures in copper polycrystal and multicrystal strained in second and third hardening stages. Evolution of the corresponding mean cell diameter with temperature.

Fig. 12. Dislocation substructures observed in Ni-20wt.%Cr alloys. (a) $t/d > (t/d)_c$, stage II ; (b) $t/d < (t/d)_c$, stage II ; (c) $t/d < (t/d)_c$, stage III (room temperature).

Fig. A1. Comparison between experimental and numerical predicted tensile curves for nickel samples (t/d = 4) and two temperatures: 203 K and 573 K.